2024 IEEE/RSJ International Conference on Intelligent Robots and Systems (IROS)
October 14-18, 2024. Abu Dhabi, UAE

Design and Modeling of a Thin-walled Multi-segment Continuum Robotic Bronchoscope

Gui-Bin Bian[1], Ming-Yang Zhang[1], Qiang Ye[1], Han Ren[1], Yu-Peng Zhai[2], Ruichen Ma[1], Zhen Li[1]

***Abstract*— Cable-driven continuum robots in bronchoscopic procedures hold immense potential to revolutionize the diagnosis and treatment of lung cancer. However, robotic bronchoscopes in current studies are typically large in size and inflexible. Therefore, this article introduces a novel cable-driven continuum robot bronchoscopy system that achieves modular design between the actuation and operation ends. A continuum structure with a dual-segment notched flexible skeleton, featuring a wall thickness of 0.45 mm, has been designed to perform bending movements exceeding 190°. This enhances flexibility and increases the spatial capacity of the working channels. A kinematic model was developed, integrating the actuation force and the mechanical characteristics of the driving cables for error compensation, estimating the correlation between the displacement of the driving cables and the position of the continuum robot's end-effector. The verification showed that the root mean square error (RMSE) of the end-effector position is 2.57 mm, which accounts for 4.8% of the continuum's length. A prototype of the robotic bronchoscopy system was created, and its performance and potential applications in bronchoscopic intervention surgeries were validated through vivo pig intervention experiments.**

I. INTRODUCTION

A. Background

With the rapid development of robotics in the past decades, its application in the medical field has become a hot research topic. Particularly in minimally invasive procedures, robotics has demonstrated its unique advantages in being able to perform complex surgical operations without causing significant trauma to the patient [1]. Cable-driven continuum robots, with their unique structural design, can mimic the continuous and flexible movements of biological entities in nature, surpassing traditional rigid robots in motility within narrow or complex environments [2]. Among the many applications, bronchial interventional surgery is a challenging area that requires extreme precision and maneuvering flexibility in order to navigate through the narrow and complex human bronchus. Due to size limitations, conventional bronchoscopes typically can only reach the 3rd or 4th level bronchi, unable to inspect or sample lesions deeper within [3]. Therefore, the design and development of a flexible continuum robot that can be precisely controlled and flexibly maneuvered is important to improve the success and safety of bronchial interventional procedures [4]. This helps to improve the success rate of early screening for lung cancer [5].

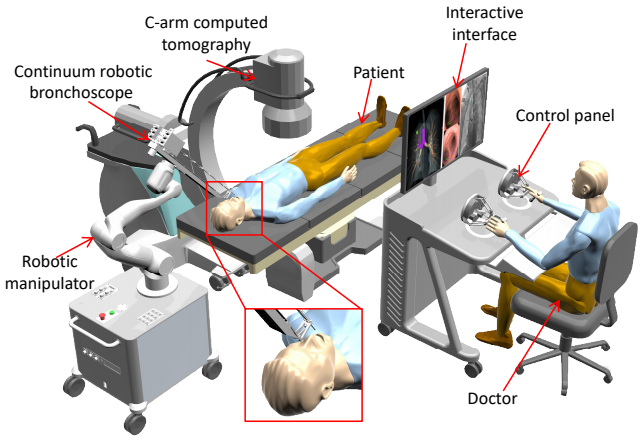

Fig. 1. Schematic diagram of the working environment of a continuum robotic bronchoscope.

B. Related Studies

The design of the operational end structure of the robotic bronchoscope is key to the effectiveness of bronchial interventions [6]. There are mainly two types of continuum robot structures commonly used due to the central working channel: one is the continuum with discrete joints, formed by the articulation of multiple joints, usually with holes on each joint for the driving cables to pass through [7]. Another method involves using nickel-titanium (Ni-Ti) elastic tubes and cutting parallel notches to facilitate bending, primarily composed of a flexible skeleton and discrete disc segments [8]. This utilizes the skeleton's own deformation to achieve movements such as bending and rotation. Zuo [9] *et al.* introduced a continuum robot made up of flexible hinges and disc structures. It has an outer diameter (OD) of 2.7 mm and an inner diameter (ID) of 1.9 mm, but a significant issue arises with large deflection angles leading to cumulative errors and changes in the focal plane position. Gao [10] *et al.* designed a flexible instrument compatible with the working channel of conventional bronchoscopes, made from thin-walled stainless steel tubes shaped by laser forming into

*This research is supported by the National Natural Science Foundation of China (Grant 62027813, U20A20196), the National Key Research and Development Program of China (Grant 2022YFB4702900), the Beijing Natural Science Foundation(L232038), the Beijing Science Fund for Distinguished Young Scholars (JQ21016), the Excellent member of CAS Youth Innovation Promotion Association (Y2022054).

Corresponding author: Gui-Bin Bian.

[1]Gui-Bin Bian, Ming-Yang Zhang, Qiang Ye, Han Ren, Ruichen Ma and Zhen Li, China and Institute of Automation, Chinese Academy of Sciences, Beijing, 100190, China. (guibin.bian@ia.ac.cn; zhangmingyang2024@ia.ac.cn; qiang.ye@ia.ac.cn; renhan.casia@gmail.com; maruichen2016@ia.ac.cn; zhen.li@ia.ac.cn)

[2]Yu-Peng Zhai, School of Automation, Beijing Information Science and Technology University, Beijing, 100096, China. (2022020419@bistu.edu.cn)

a series of discrete interlocking segments, but with limited degrees of freedom. Khadem [11] *et al.* proposed a novel bronchoscope robot for distal lung sampling, which possesses 7 degrees of freedom, controlled by 6 driving cables. The actuator is composed of a silicone tube mainframe and a driving wire fixation plate, with an OD of 4.5 mm and an ID of 2 mm. The maximum bending angle is 100°. Coemert [12] *et al.* and colleagues designed a continuum robot with an outer diameter of 3.3 mm and an inner diameter of 1.7 mm. The required working channel was machined directly into a Ni-Ti rod, and transverse grooves were engraved using laser cutting. Duan [13] *et al.*and others proposed a 3 DOF bronchial intervention robot, actuated by driving tendons threading through discrete disc segments. It has an OD of 3.2 mm and a working channel ID of 1.4 mm.

In summary, due to the specificity of bronchial interventions, a bending capability of more than 180° is typically required to reach and operate in the upper lobes of the lungs. Existing research demonstrates certain limitations in terms of terminal continuum size, tool compatibility, and flexibility. This paper proposes a dual-segment continuum robot with a thinner wall thickness, which can enhance the utilization rate of limited dimensions, increase the workspace of the working channel, and facilitate operation. Fig. 1 illustrates a schematic of the designed robotic bronchoscope intervention for oral sampling.

C. Contributions

The main contributions of this article are: 1) A continuum robot bronchoscope with a thinner wall thickness was proposed. 2) A kinematic model incorporating the mechanical properties of the driving cables was constructed. 3)The mechanism's performance was validated through representative posture experiments and application scenario tests.

II. Mechanical Structural Design

A. Robotic Bronchoscopy System Design

The robotic bronchoscope is fixed on a robotic arm, which is used to adjust the entrance operation angle. In order to meet the need for sterilization in the surgical environment, the designed robotic bronchoscope mainly consists of a continuum module a drive module, and a guide module. Among them, the drive module consists of a bending drive module and a progressive drive module. The continuum module is fixed to the bending drive module through a slot, which can realize rapid disassembly. The robot has a total of seven DOFs, including six bending modules to drive the tensile DOF of the drive line and the overall progressive drive DOF. As shown in Fig. 2, in which the progressive drive module adopts a servomotor to drive the synchronous belt movement, the delivery stroke of 550 mm. the bending drive module adopts a synchronous belt crimping plate and a synchronous belt, and the fixed connection of the delivery drive module, the continuum module and the bending drive module together under the action of progressive drive module to achieve the driving movement. The continuum module and the bending drive module together realize the pushing

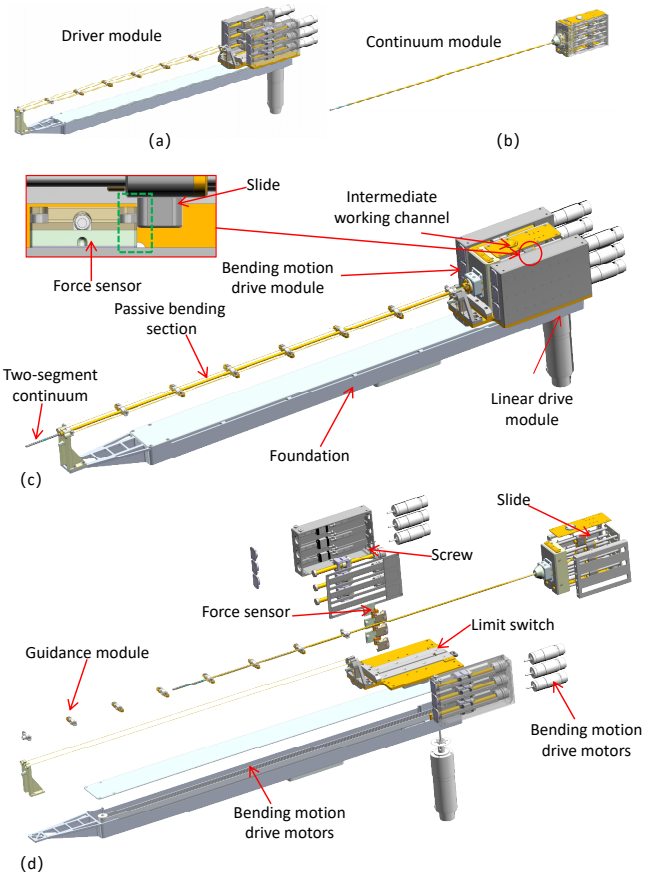

Fig. 2. Structural design of a continuum robotic bronchoscopy system. (a) Schematic diagram of driver module. (b) Schematic diagram of continuum module. (c) Schematic diagram of the overall structure of the robot. (d) Schematic diagram of each module assembly.

movement under the action of the progressive drive module. The bending drive module adopts a motor-driven screw and slider movement structure. At the same time, a slide rail is installed on the side wall of the housing to ensure the direction of movement. A tension sensor is fixed on the slider, which is in contact with the slider in the continuum module to measure the tension force of the drive cables in real-time.

B. Continuum structure design

To ensure the flexible continuum robot can navigate the complex, winding spaces of the lung's bronchi, a dual-segment flexible continuum robotic arm structure is utilized for its agility. Illustrated in Fig. 3, the design comprises two flexible segments, three guide cable discs, and several spacer discs in series. Based on the structural analysis of human bronchial deconvolution [14], the structural parameters of the designed two-segment continuum robot are shown in Table I. The proximal flexible segment is controlled by three proximal drive cables, evenly spaced at 120° intervals around the circumference, similar to the distal segment, which is controlled by three distal drive cables that pass through the proximal segment. The drive cables, made from high-hardness stainless steel cable with a diameter of 0.15 mm,

TABLE I

ROBOT DESIGN REQUIREMENTS

Parameters	indexes
ID	2.60 mm
OD	3.50 mm
Drive cable diameter d	0.15 mm
Continuum length	54 mm
Maximum bending angle	190°
Rotation dimension	Full-dimensional bending
Push trip volume	550 mm

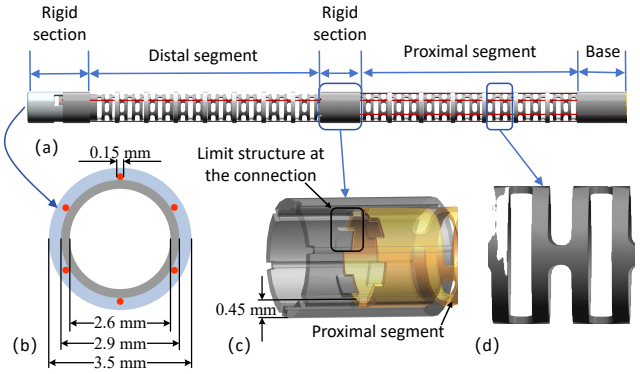

Fig. 3. Schematic diagram of the continuum structure. (a) Continuum structure. (b) End view. (c) Rigid section and flexible segment assembly structure. (d) Ni-Ti skeleton notched beam structure.

allow the continuum with an OD of 3.5 mm and an ID of 2.6 mm. This channel accommodates endoscopes and various miniature surgical tools like cell brushes, biopsy forceps, aspiration needles, tissue drills, and cell scrapers, enabling the extraction of diagnostic samples from lung nodules.

In the continuum, the incision-style flexible framework consists of a Ni-Ti alloy skeleton that is integrally formed through laser cutting. The structure of the incision beams is arranged in a staggered 90° pattern along the axial direction, utilizing the superelasticity of the Ni-Ti alloy to facilitate the bending motion of the continuum mechanical arm. The inside of the rigid section features a slotted structure serving as a limiting channel for the drive cable. The rigid section have grooves to prevent the relative rotation of parts on either side of the section. The end of the driving cable at the far end is fixed to the terminal rigid section, while the near end of the driving cable is attached to an intermediate transition ridig section. The other ends of both the far and near driving cables are secured to bolts within the bending drive module. Due to the use of thinner NiTi skeleton and rigid section, and by repurposing the path of the drive cable with the wall thickness of the rigid sections, the overall wall thickness is only 0.45 mm. This is the optimal result under the condition of ensuring structural strength.

The passive segment consists of two helical tubes with opposite directions. The inner helical tube has an OD of 2.8 mm and an ID of 2.6 mm, while the outer helical tube has an OD of 3.5 mm and an ID of 3.4 mm. Six NiTi tubes with an OD of 0.26 mm and an ID of 0.2 mm are distributed at 60° intervals between the two helical tubes, serving as channels

TABLE II

PARAMETERS OF KINEMATICS

Parameter	Meaning
j	Serial number from the proximal to the distal end of the notch continuum manipulator
i	Index number of the drive cable
α_j	Bending plane orientation angle
θ_j	Bending angle
Δl_{ji}	Stretch of the ith drive filament of the jth segment
s_t	Length of the tth rigid segment
r	Distance from drive cable center to shaft center

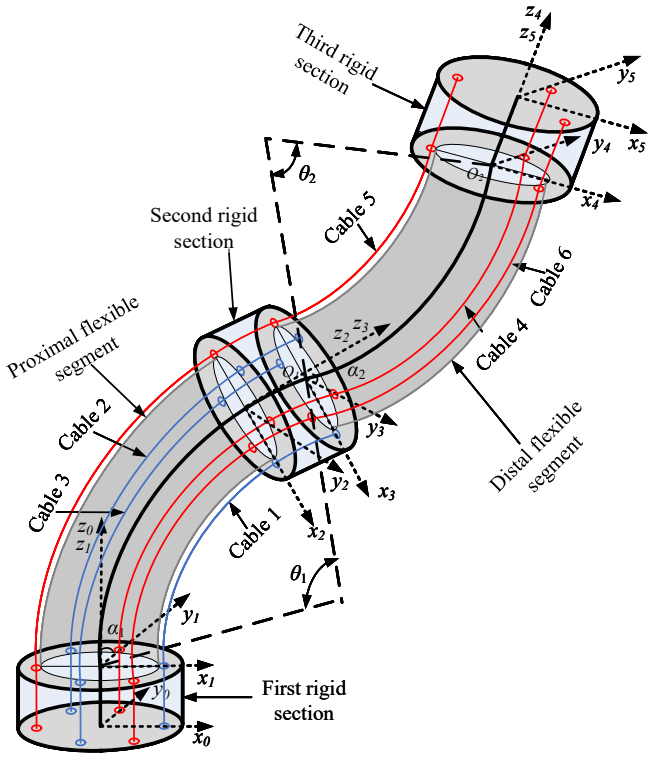

Fig. 4. Geometric modeling of a two-segment continuum.

for the driving cables to prevent interference between them. Lubricant is also applied to the driving cables to reduce friction.

III. MODELING

A. Kinematic model

In order to establish the kinematic model of the two-segment continuum, the segmented constant curvature model is used to establish the kinematic model according to the geometric properties of the continuum robot. The two-segment continuum consists of two single-segment continuums and three cable-guide disk translation segments connected in series. The geometric model is shown in Fig. 4. Some parameters are given in Table II. The coordinate systems are set up as follows: a base coordinate system is established at the bottom center of the first translation segment O_0, a coordinate system is established at the bottom center of the proximal segment continuum O_1, a coordinate system is established at the bottom center of the second translation

segment O_2, a coordinate system is established at the bottom center of the distal segment continuum O_3, a coordinate system is established at the bottom center of the third translation segment O_4, and a coordinate system is established at the center of the end of the flexible continuum arm O_5. The x-axis of the coordinate system is directed towards one of the three drive cables, the z-axis is directed along the axis, and the y-axis is determined by the right-hand rule. The transformation from an even to an odd coordinate system is a translation change and the transformation matrix can be expressed as:

$$ {}^{2j}_{2j-1}\mathbf{T} = \begin{bmatrix} 1 & 0 & 0 & 0 \\ 0 & 1 & 0 & 0 \\ 0 & 0 & 1 & s_t \\ 0 & 0 & 0 & 1 \end{bmatrix} \tag{1} $$

The transformation from an odd coordinate system to an even coordinate system is the transformation matrix for a single-segment continuum from the start point to the end point, which can be represented as:

$$ {}^{2j-1}_{2j}\mathbf{T} = \begin{bmatrix} {}^{2j-1}_{2j}\mathbf{R}_{3\times3} & {}^{2j-1}_{2j}\mathbf{P}_{3\times1} \\ 0 & 1 \end{bmatrix} \tag{2} $$

where $\mathbf{R}$ is a 3×3 matrix representing rotation, and $\mathbf{P}$ is a 3×1 column vector representing translation, indicating the end position of a single-segment continuum.

$$ {}^{2j-1}_{2j}\mathbf{R} = \begin{bmatrix} \mathrm{c}^2\alpha_j\mathrm{c}\theta_j + \mathrm{s}^2\alpha_j & \mathrm{c}\alpha_j\ \mathrm{s}\alpha_j\mathrm{c}\theta_j - \mathrm{c}\alpha_j\ \mathrm{s}\alpha_j & \mathrm{c}\alpha_j\ \mathrm{s}\theta_j \\ \mathrm{c}\alpha_j\ \mathrm{s}\alpha_j\mathrm{c}\theta_j - \mathrm{c}\alpha_j\ \mathrm{s}\alpha_j & \mathrm{s}^2\alpha_j\mathrm{c}\theta_j + \mathrm{c}^2\alpha_j & \mathrm{s}\alpha_j\ \mathrm{s}\theta_j \\ -\mathrm{c}\alpha_j\ \mathrm{s}\theta_j & -\mathrm{s}\alpha_j\ \mathrm{s}\theta_j & \mathrm{c}\theta_j \end{bmatrix} \tag{3} $$

$$ {}^{2j-1}_{2j}\mathbf{P} = \begin{bmatrix} l_j\mathrm{c}\alpha_j\left(1-\mathrm{c}\theta_j\right)/\theta_j \\ l_j\ \mathrm{s}\alpha_j\left(1-\mathrm{c}\theta_j\right)/\theta_j \\ l_j\ \mathrm{s}\theta_j/\theta_j \end{bmatrix} \tag{4} $$

where c denotes cos, and s denotes sin.

B. Drive cable movement

When the target bending angle and rotation angle are known, the movement amount of the bending drive motor is calculated as $(\Delta l_1, \Delta l_2, \Delta l_3, \Delta l_4, \Delta l_5, \Delta l_6)$, where $(\Delta l_1, \Delta l_2, \Delta l_3)$ is the actuation amount of the proximal continuum robotic arm, and $(\Delta l_4, \Delta l_5, \Delta l_6)$ is the actuation amount of the distal continuum robotic arm. The end-effector requires full-dimensional steering capabilities, hence, its movement involves the decoupled analysis of multiple segments. When the proximal continuum robotic arm performs bending and rotation movements, the distal continuum robotic arm needs to consider the coupling effect of the proximal end to maintain a stationary state relative to the proximal end. $(\Delta l_{14}, \Delta l_{15}, \Delta l_{16})$ represents the stretch amount of each driving cable of the distal driving cable affected by the bending coupling effect of the proximal continuum robotic arm. When the distal continuum robotic arm performs bending and rotation movements, it does not produce a coupling effect on the driving cables of the proximal continuum robotic arm. Therefore, the mapping of the continuum rotation angle, bending angle, and the change amount of the driving cable is as follows:

$$ \begin{cases} \Delta l_1 = \Delta l_{11} = r\theta_1 \cos\alpha_1 \\ \Delta l_2 = \Delta l_{12} = r\theta_1 \cos\left(\alpha_1 + \frac{2\pi}{3}\right) \\ \Delta l_3 = \Delta l_{13} = r\theta_1 \cos\left(\alpha_1 + \frac{4\pi}{3}\right) \\ \Delta l_4 = \Delta l_{14} + \Delta l_{24} = r\theta_1 \cos\left(\alpha_1 + \frac{\pi}{3}\right) + r\theta_2 \cos\left(\alpha_2 + \frac{\pi}{3}\right) \\ \Delta l_5 = \Delta l_{15} + \Delta l_{25} = r\theta_1 \cos\left(\alpha_1 + \pi\right) + r\theta_2 \cos\left(\alpha_2 + \pi\right) \\ \Delta l_6 = \Delta_{16} + \Delta l_{26} = r\theta_1 \cos\left(\alpha_1 + \frac{5\pi}{3}\right) + r\theta_2 \cos\left(\alpha_2 + \frac{5\pi}{3}\right) \end{cases} \tag{5} $$

Due to the long flexible segment of the bronchoscopy intervention robot, the elongation of the driving cable is a non-negligible factor. Fig. 5 shows the stress-strain curve of the 0.15 mm stainless steel cable used. The left axis corresponds to strain, and the right axis corresponds to fitted error.

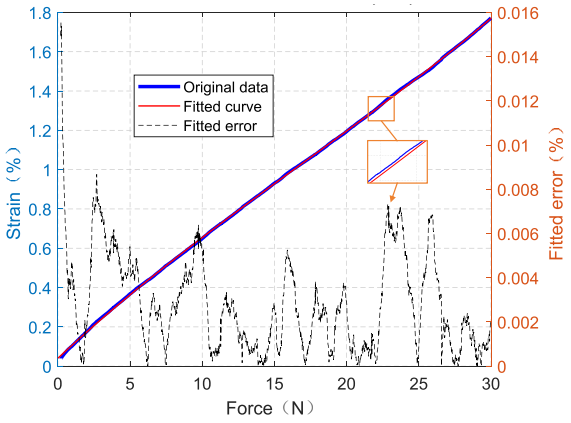

Fig. 5. Stress-strain and fitted error curve of the 0.15 mm stainless steel cable.

The expression for curve fitted is:

$$ \varepsilon_i = 0.0304 + (0.0773 \times F_i) - \left(0.0027 \times {F_i}^2\right) + \left(0.0002 \times {F_i}^3\right) \tag{6} $$

where ε_i is the strain of the driving cable under force F_i. It can be seen that the use of polynomial curves can accurately fit the stress-strain situation of 0.15mm stainless steel wire

The elongation amount A of the driving cable is calculated in real-time by measuring the tension in the driving cable with a force sensor, and this elongation is compensated into the movement amount of the driving cable:

$$ \Delta L_i = L_i \times \varepsilon_i \tag{7} $$

$$ \Delta l_i' = \Delta l_i + \Delta L_i \tag{8} $$

where ΔL_i is the elongation of the ith drive cable. L_i is the length of drive cable. $\Delta l_i'$ is the total drive cable movement.

IV. Experiments and Results Analysis

A. Experiments setup

To validate the movement capabilities and control effects of the proposed bronchoscope robot, a prototype of the continuum robotic bronchoscope was constructed. The experimental system as Fig. 6, includes the robotic bronchoscope,

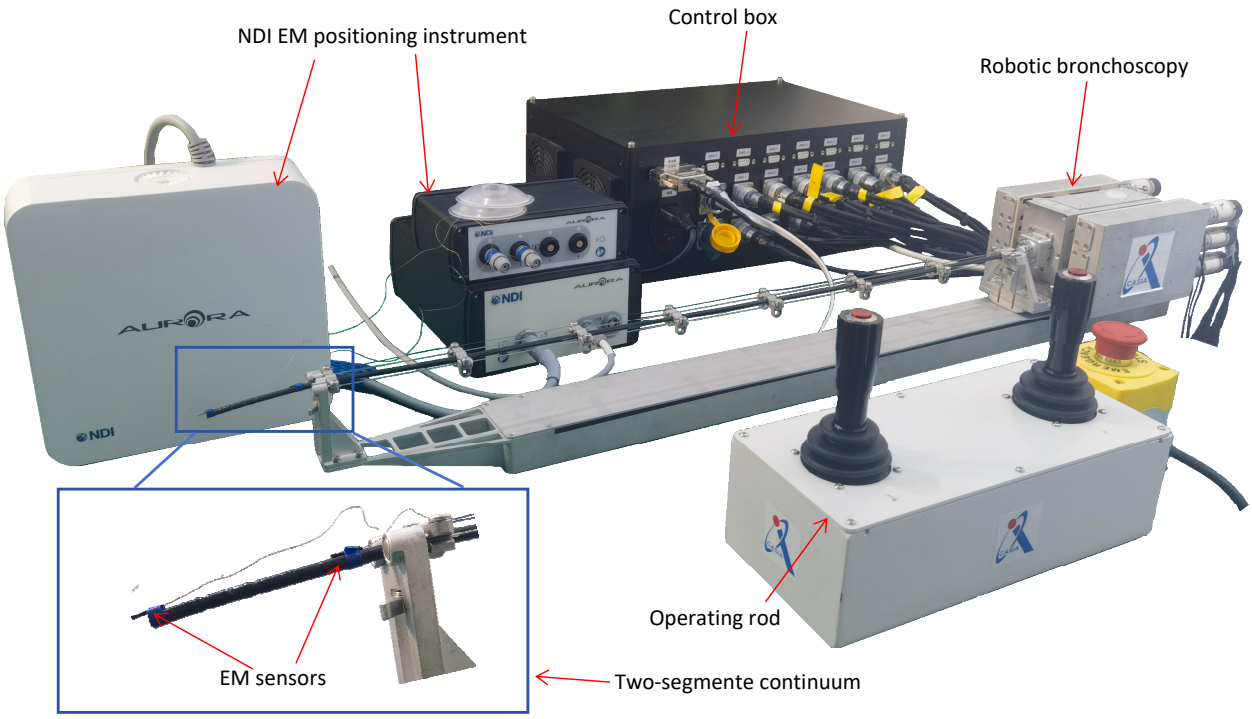

Fig. 6. Experiments platform.

control joysticks, a control box, and an electromagnetic (EM) tracker (NDI®, Canada). Two joysticks control the bending angle and direction of the two segments of the continuum, respectively. The control box connects all servo motors, force sensors, and joysticks. The controller within reads the analog signals from the joysticks to calculate the kinematics of the two continuum segments and controls the motion of the motors. Two EM sensors are placed at the base and the end of the continuum, respectively. Position information is recorded by a computer. Based on the stress-strain fitting curve for the stainless steel cable, a pre-tension force of 300 mN is applied to each driving cable before motion to prevent negative strain. Experiments to verify the bending capabilities and control effects of the robot were conducted, including in vivo pig experiments, to validate its practicality in real-world scenarios.

B. Free state bending capacity

To validate the bending capabilities of the dual-segment continuum, bending motions in four directions—upwards, downwards, left, and right—were performed. Fig. 7 shows the bending motion effects in these four directions, indicating that the dual-segment continuum robotic arm can achieve large-angle bending motions of approximately 190°. This validates that the designed continuum robotic arm has the capability for full-dimensional, large-angle bending movements, demonstrating its potential to navigate narrow and complex cavities.

C. Continuum end positioning error

EM sensors were placed at the end of the dual-segment continuum and at the base of the continuum to record position information, comparing the end-effector position from the kinematic model with the actual end-effector position coordinates.

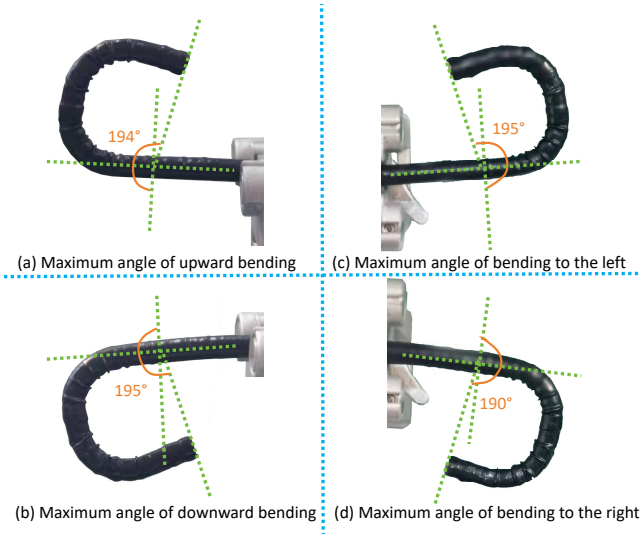

Fig. 7. Maximum bending angle of a two-segment continuum in different directions. (a) Maximum angle of upward bending. (b) Maximum angle of downward bending. (c) Maximum angle of bending to the left. (d) Maximum angle of bending to the right.

In the working space of the continuum robotic arm, the bending angles of the two segments were fixed at 30° each, totaling 60° of bending, which is consistent with most scenarios during bronchoscopic interventions [15]. The rotation angle was varied from 0-360°, resulting in a circular trajectory for the end-effector. The motion trajectory of the

continuum robotic arm is shown in Fig. 8, with the red representing the expected trajectory and the blue representing the actual trajectory, indicating some discrepancies between the actual and expected trajectories. The RMSE of the Euclidean distance for the continuum end-effector in the x, y, and z directions is 1.22 mm, 1.76 mm, and 1.41 mm, respectively. The total RMSE of the Euclidean distance between points on the expected trajectory and the actual trajectory is 2.57 mm, which is approximately 4.8% of the continuum's length.

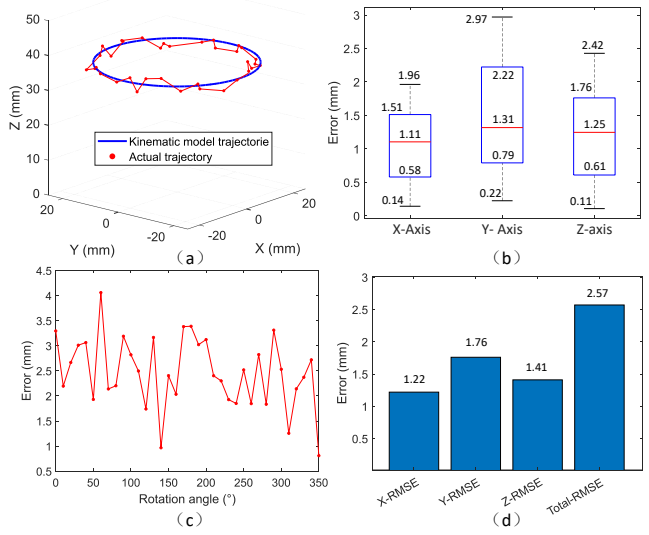

Fig. 8. Continuum end-effector positioning experiment. (a) Comparison of model trajectory and actual trajectory. (b) The boxplots of every axis error. (c) Euclidean distance error between actual and modeled trajectories for different rotational directions. (d)RMSE along every axis and overall.

The experimental results demonstrate the effectiveness of the kinematic model. The sources of error are primarily attributed to the placement error of the EM sensors and the influence of friction on the driving cables, leading to discrepancies between the actual elongation and the strain fitting curve.

D. Vivo pig intervention experiment

To verify the practicality of the proposed continuum robotic bronchoscope in real interventional scenarios, a vivo pig intervention experiment platform was established. As shown in Fig. 9(a), the vivo pig with body weights similar to adult humans was selected to simulate the real human bronchial volume. The pigs were anesthetized and the intervention was performed through the mouth. Pre-operative CT was used to segment the bronchial structure and register it with the actual scenario. Detailed navigation methods are not the focus of this paper and are not introduced. An endoscope was placed in the central working channel of the robot, and the computer displayed the endoscope images in real-time. Fig. 9(b) shows the process of selecting and entering a target branch in the bronchus. The reach can extend to the 6th to 7th bronchial levels, surpassing the range of traditional bronchoscopes. According to the endoscopic images and global position navigation, the joystick is actively used to select bronchial bifurcations. The application of this experimental platform allows for in-depth analysis and assessment of the designed robot's performance in surgeries similar to real human lung interventions, verifying the robot's steering capability and flexibility. This provides important foundational data and experience for future clinical applications.

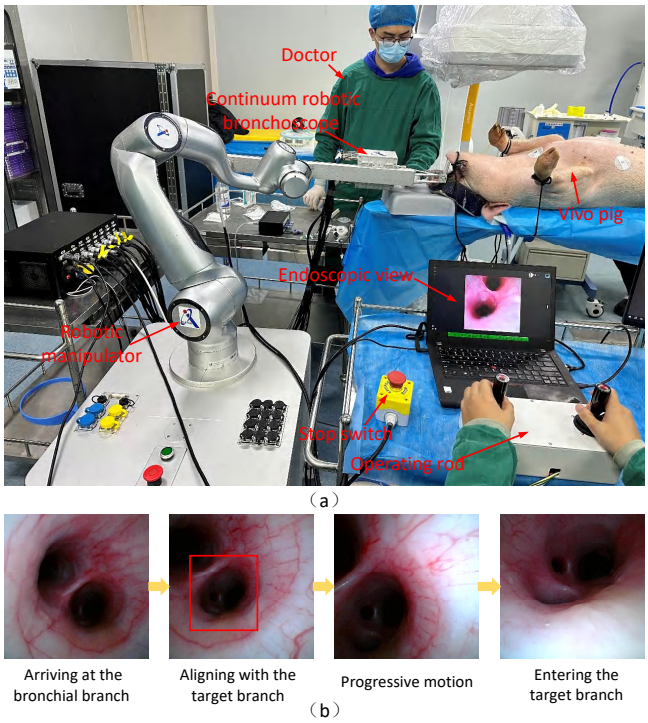

Fig. 9. Intervention experiment. (a) Vivo pig intervention experiment scenario. (b) Selecting a target branch in the bronchus and entering it.

V. CONCLUSIONS AND FUTURE RESEARCH

This study proposed an innovative cable-driven continuum robotic bronchoscopy system, demonstrating significant improvements over current bronchoscopic robots in terms of size and flexibility. The robot features 7 DOFs, employing a modular design and developing a flexible skeleton with high bending capability. This not only enhances operational flexibility but also expands the spatial capacity of the working channel. Moreover, by establishing an accurate kinematic model and performing error compensation, the end-effector positioning accuracy error is 2.57 mm. The vivo pig intervention experiment demonstrated the technical feasibility of this new type of bronchoscopic robot system, also highlighting its tremendous potential in lung cancer diagnosis and treatment. In future work, further optimization of the robot's structural design will be pursued, along with research on more robust and higher precision control models, and enhancing the robot's sensing capabilities to ensure the safety and accuracy of interventional surgeries.

REFERENCES

[1] P. E. Dupont, B. J. Nelson, M. Goldfarb, B. Hannaford, A. Menciassi, M. K. O'Malley, N. Simaan, P. Valdastri, and G.-Z. Yang, "A decade

retrospective of medical robotics research from 2010 to 2020," *Science Robotics*, vol. 6, no. 60, p. eabi8017, 2021.
[2] J. Burgner-Kahrs, D. C. Rucker, and H. Choset, "Continuum robots for medical applications: A survey," *IEEE Transactions on Robotics*, vol. 31, no. 6, pp. 1261–1280, 2015.
[3] T. Ishiwata, A. Gregor, T. Inage, and K. Yasufuku, "Bronchoscopic navigation and tissue diagnosis," *General thoracic and cardiovascular surgery*, vol. 68, pp. 672–678, 2020.
[4] B. S. Chhikara and K. Parang, "Global cancer statistics 2022: the trends projection analysis," *Chemical Biology Letters*, vol. 10, no. 1, pp. 451–451, 2023.
[5] P. J. Swaney, A. W. Mahoney, B. I. Hartley, A. A. Remirez, E. Lamers, R. H. Feins, R. Alterovitz, and R. J. Webster III, "Toward transoral peripheral lung access: Combining continuum robots and steerable needles," *Journal of medical robotics research*, vol. 2, no. 01, p. 1750001, 2017.
[6] C. Li, X. Gu, X. Xiao, C. M. Lim, and H. Ren, "Compliant and flexible robotic system with parallel continuum mechanism for transoral surgery: A pilot cadaveric study," *Robotics*, vol. 11, no. 6, 2022.
[7] N. Liu, M. E. M. K. Abdelaziz, M. Shen, and G.-Z. Yang, "Design and kinematics characterization of a laser-profiled continuum manipulator for the guidance of bronchoscopic instruments," in *2018 IEEE International Conference on Robotics and Automation (ICRA)*, pp. 25–31, 2018.
[8] W. Zeng, J. Yan, X. Huang, and S. Shin Cheng, "Motion coupling analysis for the decoupled design of a two-segment notched continuum robot," in *2021 IEEE International Conference on Robotics and Automation (ICRA)*, pp. 7665–7671, 2021.
[9] Z. Ping, T. Zhang, L. Gong, C. Zhang, and S. Zuo, "Miniature flexible instrument with fibre bragg grating-based triaxial force sensing for intraoperative gastric endomicroscopy," *Annals of Biomedical Engineering*, vol. 49, pp. 2323–2336, 2021.
[10] A. Gao, N. Liu, M. Shen, M. EMK Abdelaziz, B. Temelkuran, and G.-Z. Yang, "Laser-profiled continuum robot with integrated tension sensing for simultaneous shape and tip force estimation," *Soft robotics*, vol. 7, no. 4, pp. 421–443, 2020.
[11] Z. Mitros, B. Thamo, C. Bergeles, L. Da Cruz, K. Dhaliwal, and M. Khadem, "Design and modelling of a continuum robot for distal lung sampling in mechanically ventilated patients in critical care," *Frontiers in Robotics and AI*, vol. 8, p. 611866, 2021.
[12] S. Coemert, A. Gao, J. P. Carey, M. F. Traeger, R. H. Taylor, T. C. Lueth, and M. Armand, "Development of a snake-like dexterous manipulator for skull base surgery," in *2016 38th Annual International Conference of the IEEE Engineering in Medicine and Biology Society (EMBC)*, pp. 5087–5090, 2016.
[13] X. Duan, D. Xie, R. Zhang, X. Li, J. Sun, C. Qian, X. Song, and C. Li, "A novel robotic bronchoscope system for navigation and biopsy of pulmonary lesions," *Cyborg and Bionic Systems*, vol. 4, p. 0013, 2023.
[14] M. H. Tawhai, A. Pullan, and P. Hunter, "Generation of an anatomically based three-dimensional model of the conducting airways," *Annals of biomedical engineering*, vol. 28, pp. 793–802, 2000.
[15] N. Liu, C. Bergeles, and G.-Z. Yang, "Design and analysis of a wire-driven flexible manipulator for bronchoscopic interventions," in *2016 IEEE International Conference on Robotics and Automation (ICRA)*, pp. 4058–4063, 2016.